Towards cavity-collapse hazard maps with Zeb-Revo handheld laser scanner point clouds

Thomas Dewez, Silvain Yart, Ysoline Thuon, Pierre Pannet, Emmanuelle Plat

THE PHOTOGRAMMETRIC RECORD

The Photogrammetric Record 32(160): 354–376 (December 2017)
DOI: 10.1111/phor.12223

TOWARDS CAVITY-COLLAPSE HAZARD MAPS WITH ZEB-REVO HANDHELD LASER SCANNER POINT CLOUDS

THOMAS J. B. DEWEZ* (t.dewez@brgm.fr)
SILVAIN YART (s.yart@brgm.fr)
BRGM, French Geological Survey, Orléans, France

YSOLINE THUON (y.thuon@brgm.fr)
PIERRE PANNET (p.pannet@brgm.fr)
BRGM, French Geological Survey, Reims, France

EMMANUELLE PLAT (e.plat@brgm.fr)
BRGM, French Geological Survey, Nantes, France

**Corresponding author*

Abstract

Underground cavities are ubiquitous across northern Europe's cities and countryside due to a long history of mining and building-stone extraction. Management of cavity-collapse risks requires detailed knowledge of a cavity's geometry, depth and rock-mass characterisation. Current mapping practices are neither sufficiently accurate, detailed nor cost-effective in underground settings. Here, a GeoSLAM Zeb-Revo handheld mobile laser scanner was tested. Its point clouds reproduced planes faithfully (RMS < 10 mm) over typical gallery dimensions (<10 m) and any survey horizontality defect was not measurable. In well-structured corridor networks, reference distance inaccuracy arising after a 115 m loop and 5·25 minutes of instrumental drift did not exceed 3 mm over 30 m (1:10 000) and the difference from the reference length was insignificant. Applied to mapping 11 ha of a disused underground stone quarry in the Paris Basin, Zeb-Revo surveys produced accurate (<1 m) base maps adequate for regulatory cavity hazard maps at 1/5000 scale. Geometric knowledge of accessible cavities is therefore no longer a challenge for collapse hazard mapping.

KEYWORDS: cave, handheld mobile laser scanner, lidar, mine, quarry, topographic survey

INTRODUCTION

THE COLLAPSE OF UNDERGROUND VOIDS is a common hazard in many places worldwide, where underground material has been emptied by natural processes (such as karstic caves and lava

tubes) or by industrial activities (mines, quarries) (for example, Langer, 2001; Heitfeld et al., 2006).

All through history, urban development has relied on available building material. To minimise transportation effort and costs, many building-stone quarries were dug directly underneath cities. In parallel, dwellings were built above iron and coal mines during the industrial revolution in many European towns and cities. Today, densely populated cities of the northern European coal belt, running from Wales in the United Kingdom to northern France, Belgium, Germany and Poland, are built upon previously exploited underground workings (Heitfeld et al., 2006). The countryside is also not exempt from underground cavities. The geological basins of London and Paris, for instance, are widely covered in nutrient-poor decalcified clays. Agricultural performance of this extensive farmland has long been boosted by bringing nutritious lime from 20 to 30 m deep quarries dug under the fields. Normandy alone is thought to host in excess of 76 000 such so-called *crayères*. Whatever their cause, underground voids are not stable over the long term and often collapse, generating surface damage manifested by sinkholes and ground settlement (Fig. 1) (Langer, 2001; IFSTTAR, 2014).

In the post-mining era, public authorities have endorsed the responsibility to manage underground collapse risks in order to mitigate, repair (where possible) and prevent further damage. In this endeavour, knowing (i) where the voids are with respect to surface assets; (ii) how large they are; and (iii) how deep they lie, are three key determinants to address the risk of cavity collapse (IFSTTAR, 2014). Answers to these questions are first sought in historical documents and completed by field investigations. The degree of effort expended depends on the value of the exposed assets above such workings.

For decades, mining surveyors with levels and theodolites have mapped underground cavities with success. Such techniques were slow, costly and required careful surveying skills, the results being produced as 2D line drawings. In today's state of the art, total stations remain the most accurate instrument to establish a reference system in a cavity. If cruder cavity sketches can only be afforded, underground mapping relies on surveying chain, compass-clinometer and tape measure (or distance meter). It is slower than conventional surveying, collects fewer points far less accurately, but is cheap and uses simple technology. This is currently the reference technique among speleologists.

Practitioners now express a need to enhance mapping capacity to improve cavity stability diagnostics while keeping costs under control. Beyond representing a threat, underground galleries may now become an unexpected asset because some have naturally cooling capabilities, assisting the installation of data centres. However, turning cavities into bankable assets requires accurate maps of gallery networks and their dimensions, requiring more advanced approaches.

Today, terrestrial laser scanning (TLS) or structure-from-motion (SfM) techniques perform well in the open air to determine details in rural (Dewez et al., 2013; 2016b; Vanneschi et al., 2017) or urban settings (for example, Musialski et al., 2013). Caves and mine galleries suffer from very limited lines of sight and cluttered views from any one position (Eyre et al., 2016; Cadge, 2017). Multiple measurement stations to fill shadow or occluded areas make both techniques uneconomical, even if examples exist in the literature (Hannemann et al., 2012; Roncella et al., 2012; Eyre et al., 2016; Gallay et al., 2016). Mobile laser scanning technology emerged and was developed to bridge this gap, as reported, for example, by Bosse et al. (2012), Zlot and Bosse (2014) and Baiden et al. (2014). Only a few studies describe the performance of such equipment (James and Quinton, 2014; Chan et al., 2016; Eyre et al., 2016; Vanneschi et al., 2017). All authors nevertheless agree that the rapidity with which handheld laser scanners perform in mining environments is key to

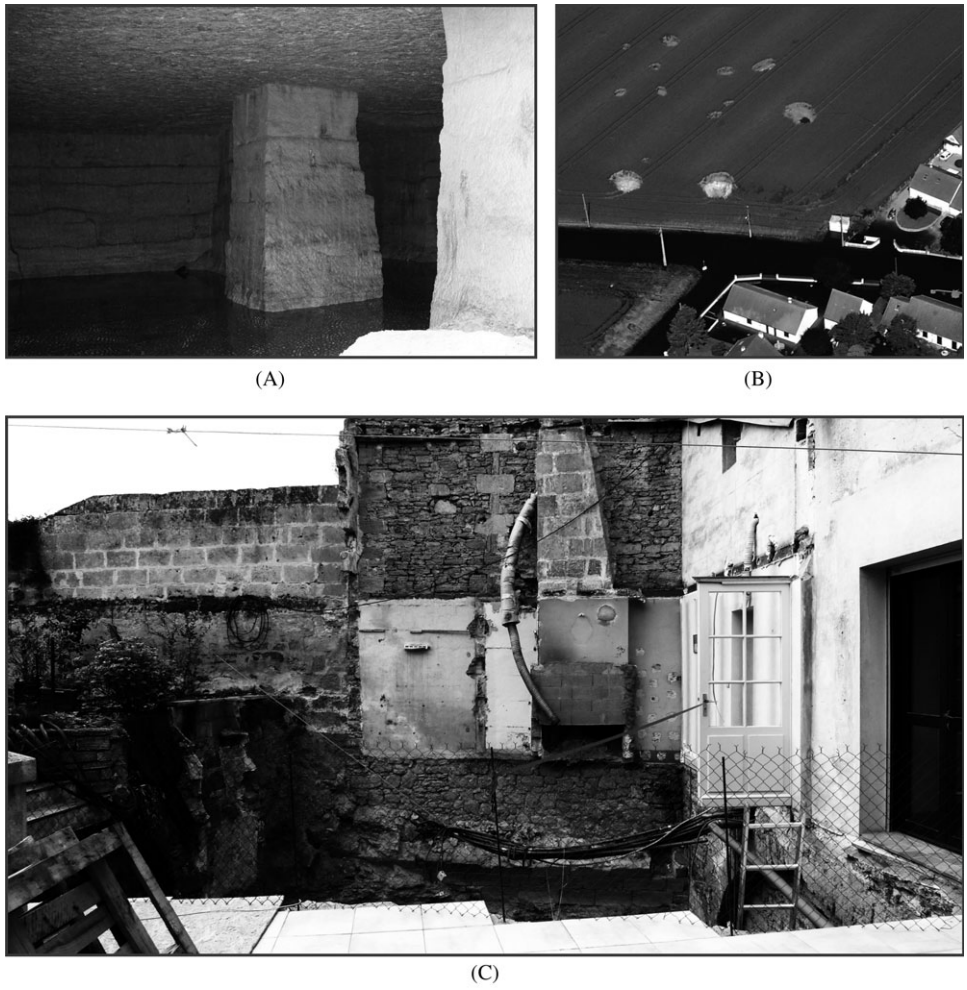

FIG. 1. (A) Building-stone underground quarry of Fleury-sur-Orne (Calvados, France) with pillars supporting the cavity roof, some reaching 10 m in height (© E. Plat – BRGM 2014). (B) Thirteen sinkholes formed following exceptional rainfall in late May 2016 in the village of Gidy, central France. These sinkholes turned out to be located above a forgotten quarry (© T. Dewez – BRGM 2016). (C) Damage caused by sinkhole collapse to a house in Doué-la-Fontaine (Maine-et-Loire, France). The extension to the main house entirely disappeared into the 400 m^3 sinkhole (© E. Plat – BRGM 2011).

keeping costs under control. The rapidity of these devices admittedly means achieving lower precision, but they remain within the limits acceptable for operational mapping.

This paper reports on experiments carried out to document the performance of a Zeb-Revo handheld mobile laser scanner (Bosse et al., 2012) and demonstrate its use in underground cavity-collapse hazard studies. The purpose is to demonstrate not only that point clouds of underground workings are visually impressive, but that they also possess most of the necessary features to build cavity-collapse hazard maps. Finally, a reflection is

proposed on the added value brought by mobile lidar point clouds compared to routine technologies employed today in collapse risk management.

Handheld Mobile Laser Scanners

Zeb-Revo handheld mobile laser scanners combine time-of-flight line scanners with an inertial navigation unit to record the spatial attitude of the scanning plane without the need for satellite navigation systems (Bosse et al., 2012). The position of walls around the scanner is determined using a simultaneous location and mapping (SLAM) algorithm (Bosse et al., 2012). SLAM algorithms assume that the scanner's surroundings are static, retain recognisable geometries and do not deform.

The Zeb-Revo rotates a Hokuyo ULM-30LX F-type scanner on an axis perpendicular to the scanner's handle. It pulses 42 300 effective points per second with an angular increment of the order of 0.006 rad (for example, 1 point every 6 mm at 1 m distance for a single sighting). Though this may seem sparse compared to conventional terrestrial laser scanners, the cloud density rapidly increases when moving through the premises (Eyre et al., 2016). Hokuyo's scanner specifications indicate that the maximum range over which the Zeb-Revo performs is 30 m. In broad daylight, this range falls off dramatically. For example, in a coastal cliff survey in Socoa (southern Atlantic coast of France), under 1% of points reached beyond 7·42 m (Fig. 2); the laser echoes were probably drowned by the ambient light. In complete darkness, however, in a tall cavity near Châlons-en-Champagne (northern France), the Zeb recorded echoes from light-coloured surfaces as far as 35 m away.

By trial and error, it was found that the scanner's own X reference system axis was normal to the scanner's back plate. When initialising the scanner in a vertical position with its back plate lined up in a north–south direction, and with the lidar head pointing east, the

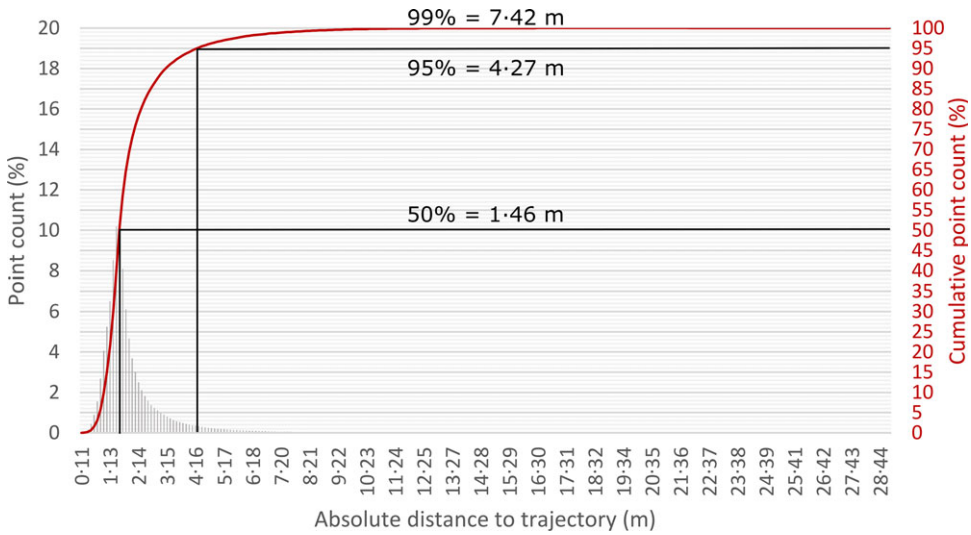

Fig. 2. Distribution of point distances from Zeb-Revo in a broad daylight outdoors cliff survey. Ninety-nine per cent of points only reached 7·42 m.

point-cloud coordinate system would line up with regular cartographic reference frames. This greatly eased cloud-to-cloud registration by removing the azimuth rotation unknown. Co-registration of point clouds was thus reduced to determining the translation to a common origin.

Zeb scanners do not record laser point intensity. Only significant geometric features can be used, either by manually selecting pairs of recognisable points between a reference cloud and a free-moving dataset (for example, Eyre et al., 2016), or by cloud-to-cloud registration using iterative-closest-point solutions (Besl and McKay, 1992).

In the following section, deeper precision and accuracy checks are discussed to document the Zeb-Revo performance. The approach addresses aspects different from those in James and Quinton (2014), Chan et al. (2016) or Eyre et al. (2016) in that possible point-cloud rigidity defects on distance measurements are also assessed.

DOCUMENTING ZEB-REVO POINT-CLOUD PRECISION AND ACCURACY

Reference Dataset

The upper floor of an office building was surveyed with a Zeb-Revo in a single loop over a volume of 32 m × 22 m × 3 m (length × width × height) (Fig. 3). The central corridor was 1·60 m wide and 2·60 m high. The corridor walls are well structured with salient or recessed sections 0·5 m deep, alternating left and right in an irregular metre-scale

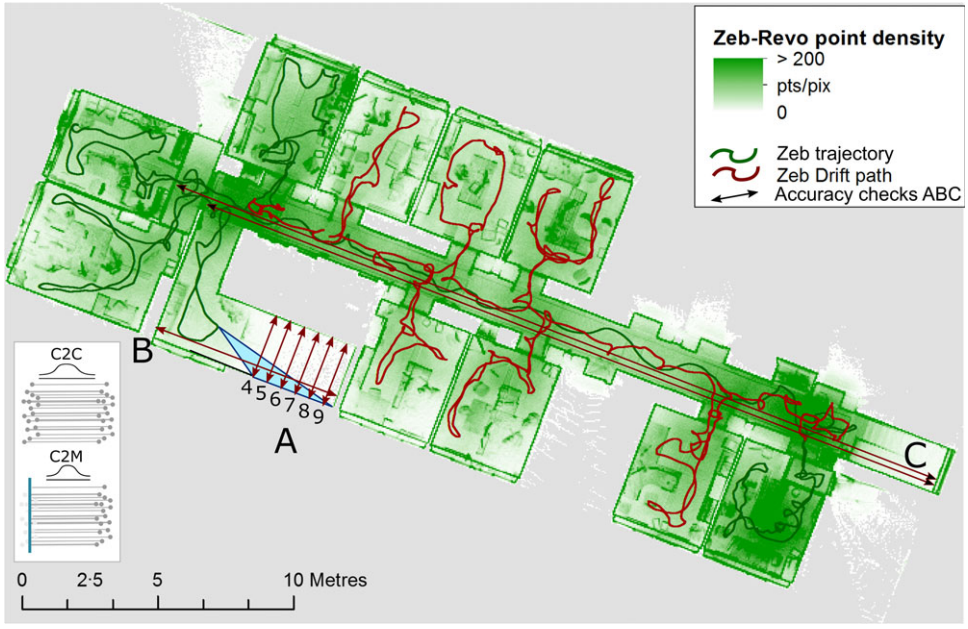

FIG. 3. Plan view of an office building floor and Zeb-Revo trajectory (dark green). The Zeb trajectory in dark red is the path tested for drift. A central corridor (1·6 m wide) leads to 10 rooms. Arrows indicate where accuracy checks were sampled. The blue wedge figures the increasing laser ray obliquity on the wall as distance increases. (A) Stairwell widths (*c*.2·370 m). (B) Stairwell lengths (*c*.7·105 m). (C) Corridor lengths (*c*.28·876 and 30·198 m). Accuracy checks on point clouds used both C2C (cloud-to-cloud) distances and C2M (cloud-to-model), where the model is the best-fit plane to one of the point-cloud subsets.

longitudinal pattern. Such structural geometry seems appropriate for testing the Zeb's precision without impacting SLAM results with smooth wall surfaces (Bosse et al., 2012).

The unfolded survey path spanned 308 m, which was walked in 11 minutes and 52 seconds at an average pace of 1·5 km/h (Fig. 3). *Median* point-cloud density was 26 700 points/m² (1 point per 6·1 mm); *mean* density was 36 000 points/m^2 (1 point per 5·3 mm). A segmented floor surface was used to test point-cloud capability to reproduce their planar geometry.

RMS Plane Distribution

Testing the plane-fitting root mean square (RMS), as performed by Chan et al. (2016), can be done in several ways. CloudCompare (cloudcompare.org) implements three methods to fit planar objects: plane fitting to a complete cloud (Tools > Fit > Plane or 2D polygon – both methods are identical), and manual plane fitting on a limited neighbourhood (Plugins > Compass). All methods report the goodness of fit with RMS values.

The plane (Fit > Plane), adjusted to the entire building floor points, had a RMS of 7·5 mm for the entire 270 m² with 2·4 million points. Although this first RMS metric could conceal a possible positional drift of the Zeb, which is discussed below, no detectable tilt of the surface came out of the data. The Zeb-Revo survey does not exhibit any residual tilt down to the eighth decimal place.

To assess short-wavelength undulations, a piecewise plane-fitting assessment should produce smaller RMS values. This was tested with 21 planes, about 1·2 m apart, sampling all floor points within a radius of 0·72 m with the plugin Compass (Thiele et al., 2017). These 21 local planes had an average RMS of $5{\cdot}9 \pm 0{\cdot}6$ mm (range: 5·3 to 7·6 mm). This value is indeed smaller than the global adjustment and produces better local plane fitting. Yet it is not known if the reduction in RMS value from the global floor plane to local planes (1·6 mm RMS difference) should be seen as the signature of the Zeb residual drift or is simply reproducing existing undulations in the concrete slab (a fringing light shone on the floor revealed that undulations exist, but their shallow amplitude could not be measured). To gain better insight into point-precision distribution, a roughness metric is used to assess surface planarity for every cloud point.

Roughness (Cross-validation as a Function of Zeb Distance)

CloudCompare defines *roughness* as the distance of one central point to the best-fit plane of its neighbours in a given search diameter (CloudCompare, 2015). This definition is a metric for cross-validating interpolations. The roughness in Fig. 4 is reported for floor points only to avoid skewing the signal with adjacent wall points. Neighbourhood diameter was increased stepwise from 1 to 10 cm. Results show that the roughness stabilises at 4.1 mm (distribution quantile at 68%; this quantile is the robust equivalent of RMS for non-Gaussian distributions) (Fig. 4) for search diameters beyond 5 cm in diameter. This spatial autocorrelation *sill* occurs crudely at 10 times the mean point spacing. The roughness amplitude itself also corresponds crudely to the point spacing.

Roughness distribution characteristics (Fig. 4) show the precision limit of SLAM algorithms using limited accuracy instruments (see the lidar specifications in Hokuyo, 2017). Acquiring denser point clouds, either with shorter Zeb-to-surface distances, or by walking the Zeb more slowly through the surveyed space, will not bring any better surface shape definition because the laser range finder and attitude sensors have limited accuracy. Oversampling will only create spurious surface morphologies (Buckley and Mitchell, 2004). In practice, unlike

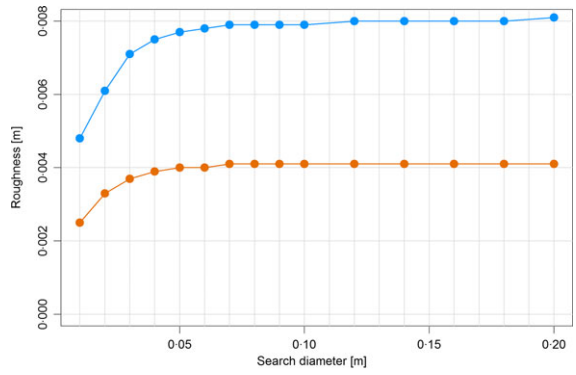

FIG. 4. Point-cloud roughness as a function of the search diameter for points located on the floor of an office building. Roughness is defined as the normal distance to the best-fit plane adjusted on a set of points surrounding a candidate. The search diameter specifies how many points enter in the plane-fitting procedure. Orange: 68% quantile of roughness (q68% is the robust statistical value equivalent to RMS in Gaussian distribution), it reaches 4.1 mm for radii greater than 4 cm. Blue: 95% quantile.

conventional TLS, where angular spacing can be set, point density is extremely difficult to anticipate during Zeb-Revo acquisition. This is because each surface can be seen many times from vastly different points of view. Nevertheless, to go beyond this precision description, this paper now examines how the point precision may be diluted with distance.

Point Dilution of Precision with Distance

The Hokuyo lidar specification sheet (Hokuyo, 2017) indicates that point positioning precision worsens with increasing distance to the scanner. To explore this dilution of precision with distance, the closest distance from the Zeb trajectory to the point cloud was computed (in the sense of cloud-to-cloud computation). Lines of sight may occasionally be longer than the closest scanner trajectory point but actual line-of-sight distances are not provided in output clouds.

Seventy-five per cent of the points surveyed in this office building lie less than 1·30 m away from the scanner. This distance, corresponding to the operator's elbow height, is unfortunate because the ceiling is 2·6 m above floor level. The only place with clear surfaces and longer direct lines of sight were located in the stairwell. There, three vertical walls in the stairwell stand between 1·35 and 5·30 m from the Zeb trajectory (Fig. 5). Wall roughness plotted against distances shows that the 68th percentile of roughness at 10 cm diameter increases with distance, but remains mostly below 10 mm. When removing the effect of distance, the 68th percentile of normalised roughness remains constant at around $2{\cdot}7 \pm 0{\cdot}8$ mm across the distance range. This can be interpreted as the roughness term being composed of a constant plus a distance-variant part. The manufacturer rates Zeb-Revo for measuring points with a precision of 5 mm + 1 mm/m. It was noticed, empirically, that this constant was smaller for the equipment used here. In well-structured indoor buildings, Zeb-Revo achieves better than half-a-centimetre precision. The next section documents the measurement accuracy.

Documenting Measurement Accuracy

Previous studies discussing the Zeb-1 performance (for example, James and Quinton, 2014; Chan et al., 2016; Eyre et al., 2016) relied on terrestrial laser scanner surveys to

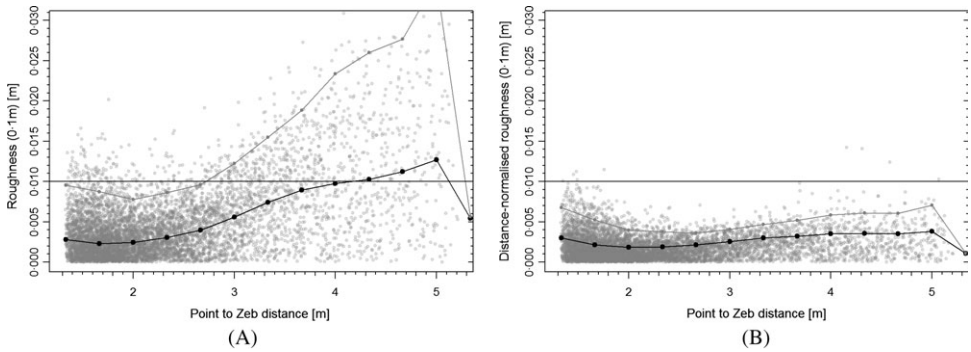

FIG. 5. Dilution of point precision with increasing line-of-sight distance from the Zeb scanner. (A) Roughness as a function of distance to the Zeb device. (B) Normalised roughness (roughness weighted by distance) as a function of distance. Normalised roughness stays constant throughout the distance range at $2{\cdot}7 \pm 0{\cdot}8$ mm. Roughness is assessed for neighbourhood diameters of 10 cm. Black points and line represent the 68th roughness percentile (equivalent to RMS); grey points and line represent the 95th roughness percentile.

provide abundant accurate reference data. This research, unfortunately, did not have access to a terrestrial laser scanner to control the surveys. Instead, accuracy control was performed using much sparser measurements acquired with two electronic distance meters: a Leica Disto D210 with a calibration certificate quoting $\pm 0{\cdot}2$ mm in the range 0·1 to 7·8 m, and a Bosch PLR-30 which, although putatively less accurate, was used to detect possible blunders.

Validation of distances extracted from the Zeb-Revo survey were performed in the stairwell of the building and in the main corridor where direct lines of sight were longer than 1·30 m (Table I). Stairwell width was controlled with three measurements at each staircase step at operator shoulder height (about 1·50 m). Disto measurements are coherent within $\pm$ 0·5 mm of each other along the entire staircase. Zeb-Revo point-cloud distances were assessed using a cloud-to-mesh metric. Patches of walls corresponding to the reference distance were segmented numerically with height above the ground and distance to a reference wall. The wall on the opposite side of the staircase was modelled as a best-fit plane (RMS = 0·005 m). In Table I, the stairwell width in A shows that distance accuracy varies systematically with increasing Zeb distance. This is a hidden effect of line-of-sight obliquity; as this obliquity becomes shallower (from 28° to 18°), the measured width diminishes at a rate of 4 mm/m (1/250). On the other hand, when lines of sight are orthogonal to the wall surface (Table I, B stairwell length), distance accuracy remains excellent at longer ranges. Here, an insignificant distance error of 1·6 mm is observed over 7·1 m, which makes a relative distance accuracy of 1/5000 even though this 7·10 m distance was deduced from two SLAM-combined lines of sight.

Testing the Accuracy of the SLAM Solution

The final verification targeted possible cumulative errors from the SLAM solution, which would result in point-cloud deformation and betray a lack of reference-frame rigidity. The longest direct lines of sight of the main corridor were chosen, with end wall surfaces that were never measured at once from a single station (lengths C in Fig. 3). Points representing these surfaces were selected based on their time-stamp labels of 105 and 420 s

TABLE I. Zeb-Revo precision and accuracy checks in an office building (locations in Fig. 3). Control distances were acquired with Leica Disto D210 and Bosch PLR-30 distance meters. A, B and C refer to different control configurations:
A. Accuracy of distances between walls with direct Zeb lines of sight. Accuracy degrades with line-of-sight obliquity.
B. Distance accuracy for walls reconstructed from SLAM-dependent Zeb positions (near instantaneous). When Zeb lines of sight are orthogonal to wall surface, distance accuracy is four times better for distances 75% longer.
C. Accuracy control for distances dependent on SLAM accuracy. Distance accuracy remained better than 3 mm over *c*.30 m (that is, 1/10 000 relative accuracy).

	Leica Disto D210			*Bosch PLR-30*			*Distance cloud to model (plane)*				*Accuracy*		
	Mean (m)	*SD* (m)	*Nm* (–)	*Mean* (m)	*SD* (m)	*Nm* (–)	*Mean* (m)	*SD* (m)	*Npts* (–)	*Surface area* (m^2)	*Distance to Zeb* (m)	*Zeb-Disto* (m)	*Obliquity* (°)
A. Stairwell width													
Reference plane RMS = 0·00072 m													
Step 4	2·3710	0·0000	3	2·3703	0·0005	3	2·3712	0·0043	164	0·116	2·42	0·0002	28
Step 5	2·3710	0·0000	3	2·3713	0·0005	3	2·371	0·0047	145	0·129	2·70	0·0000	26
Step 6	2·3713	0·0005	3	2·3707	0·0005	3	2·3689	0·0056	90	0·123	3·01	−0·0024	23
Step 7	2·3693	0·0005	3	2·3700	0·0008	3	2·3674	0·0074	66	0·115	3·34	−0·0019	21
Step 8	2·3683	0·0005	3	2·3690	0·0000	3	2·3639	0·009	44	0·107	3·67	−0·0044	20
Step 9/landing	2·3653	0·0005	3	2·3663	0·0005	3	2·3582	0·0099	97	0·541	4·05	−0·0071	18
											Average	**−0·0026**	
											SD	**0·0028**	
B. Stairwell length													
Reference plane RMS = 0·00091 m	7·1045	0·0018	6	7·104	0·002	6	7·1061	0·0094	681	0·576	5·046	**0·0016**	
C. Corridor lengths													
Door lintel to upper lintel	28·8740	0·0010	15	28·870	0·001	3	28·8763	0·0017	364	0·117[a]		**0·0023**	
Wall to lower lintel	30·1980	0·0010	15	30·198	0·005	3	30·2009	0·0019	242	0·119[a]		**0·0029**	

[a]Measurement dependent on SLAM solution, both faces were measured 315 seconds apart, after 115 m of journey without direct view.
SD = standard deviation; Nm = number of measurements; Npts = number of Zeb points. Reference plane RMS: A = 7·2 mm; B = 9·1 mm; C28 = 6·3 mm; C30 = 6·3 mm.

(thus 5 minutes and 15 seconds apart), after a walk of 115 m without a view of these surfaces. Reference distances from Leica Disto D210 took 15 stacked readings of $28{\cdot}874 \pm 0{\cdot}001$ m for the first surface and $30{\cdot}198 \pm 0{\cdot}001$ m for the second one. The reference walls were modelled with RMS = 0·006 mm. Here again, Zeb point clouds reproduced the reference distances to within 3 mm over a 30 m distance, in other words with a relative accuracy of 1/10 000.

While underground quarries are much broader objects, the accuracy metrics found here can be directly applied to gallery width and height, together with the presence and dimensions of pillars. What is different is the quality of loop georeferencing, which was achieved with a network of markers surveyed by a total station with reported accuracy always better than 1 m and mostly better than 10 cm. This paper will now address the topic of cavity-collapse hazards as informed by handheld mobile laser surveys.

Cavity-collapse Risk Management and Technology

In France, engineering methods to diagnose collapse susceptibility and hazard are described in several reference documents (such as GEODERIS, 2006; Vuidart, 2012; IFSTTAR, 2014). They rely on documenting suspicions of voids and a predisposition for rupture and collapse. Both aspects are performed by skilled geotechnical engineers, supported by geometric data of varying quality and compiled in a 2·5D (flat) geographic information system. To improve the cost effectiveness of risk-management policies, better geometric description of cavities will reduce mitigation costs.

The parameters needed to assess roof stability are:

(1) the maximum roof span (width of the gallery or distance between pillars);
(2) the weight of the overburden (hence thickness of the roof horizon);
(3) the void volume available to accommodate decompressed collapse rubble;
(4) the scree slope angle; and
(5) elements' diagnostic of fragility (rock resistance, fractures, flaking, water circulation and so on).

Cavity-collapse diagnostics carried out on large sites require many days to survey and diagnose. This means examining all the locations where the cavity roof may fail and where it is not supported by pillars.

Site Survey

The study site is an underground building-stone quarry, located in the Paris Basin in northern France. Site specifics will not be described in great detail because of public sensitivity to risk management for this site. The authors' purpose is solely to describe how point clouds can be turned into input for mapping cavity-collapse hazards. Nevertheless, it should be noted that the quarry started being dug out perhaps two millennia ago, based on Roman graves using this stone being discovered in the vicinity. Despite early extraction phases, most of the stone quarrying took place from the Middle Ages onwards. Cassini historical maps from the middle of the 18th century ascertain its existence under the reign of Louis XV, around 1750. Extractive activity went on until the 20th century. While stone is no longer carved out today, abandoned blocks carved earlier and still present in the galleries may be used for building restoration. The quarry is extensive, up to 120 ha. It is a so-called *pillars-and-chambers* type quarry. Although not known with certainty, historical archive accounts indicate more than ten thousand pillars.

The laser scanning survey, as a trial example, only covered 15 ha of the quarry in a sector located underneath the village. Thirty-five loops were acquired but only 25 were registered properly together (Fig. 6). SLAM processing failed to provide 3D point coordinates for the remaining 10 loops, perhaps because of the lack of geometric features somewhere along the journey. The 25 successfully processed loops were tied to 240 conventional survey pins, materialised in 3D by signalling cones. This is to control topographic drift and deformation. The subcontracted survey company in charge of the Zeb survey estimated that the worst topographic discrepancy between the Zeb survey and the conventional survey pins never surpassed 1·0 m. Most loops were registered to better than 10 cm with respect to the conventional topographic network. Survey reports unfortunately lacked any further details.

In the 15 ha covered in four working days, not all loops could be registered to the others: in the end, only 11·1 ha (111 071 m²) were correctly registered. This yielded the reconnaissance of 1964 pillars with a surface area larger than 2 m². The Zeb generated a total dense point cloud of more than 1·1 billion points (Fig. 6). The most frequent density is about 2100 points/m² (1 point every 21·8 mm) on all floors, walls and ceilings (Fig. 7). The survey area fits into a rectangle 800 m wide by 750 m long (Fig. 6). The stone extraction took place in a single, nearly horizontal, bed. It is therefore a single-level quarry, as opposed to extraction work carried out on several levels elsewhere.

POINT-CLOUD PROCESSING

The purpose here is to describe how 3D point clouds can be turned into meaningful geotechnical information using CloudCompare, together with standard geographical

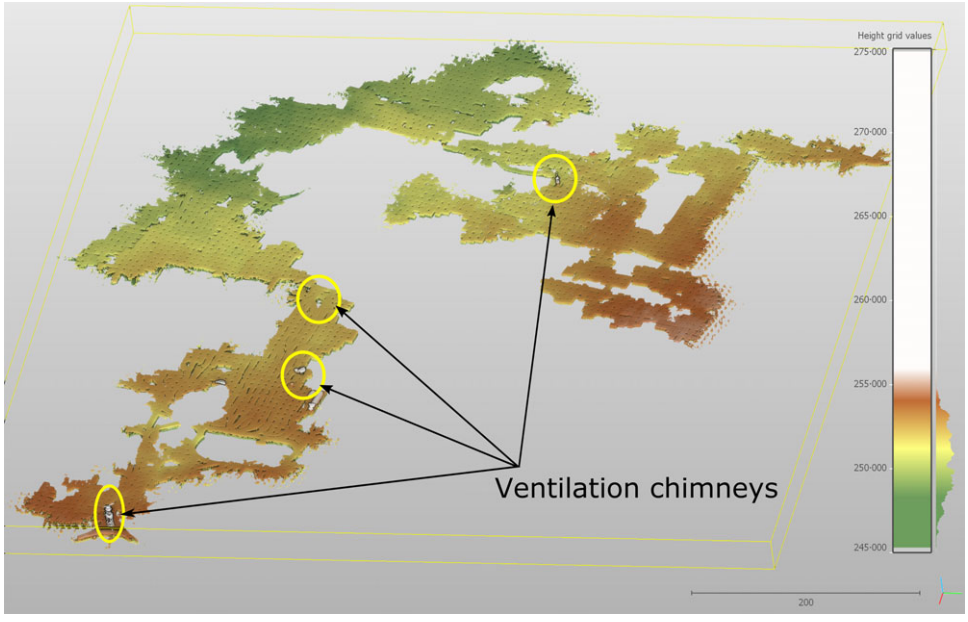

FIG. 6. Overview of the 11·1 ha of the scanned quarry. Colours depict elevation in metres. Ellipses highlight roof-collapse phenomena.

FIG. 7. Detailed view of point density (number of echoes per 10 cm × 10 cm cell) in a quarry extract. Density of 1 point/cm (score of 100 points/100 cm²) is mid-green. Darker greens show greater density. Such a view also highlights the path followed by the operator and demonstrate where geometric knowledge is best constrained.

information system (GIS) software. Processing poses two assumptions: (i) co-registration and exterior orientation to the topographic reference frame of all point clouds were applied to the dense cloud and to the scanner's head trajectory cloud; (ii) underground galleries were not necessarily dug horizontally, so processing should adapt to slanted levels which precludes such simple processing as thresholding based on the elevation coordinate. With these prerequisites, the following goals were addressed:

(1) Tagging floor, wall and ceiling clouds.
(2) Tracing the gallery 2D plan of the walls at 1 m above the gallery ground level.
(3) Tagging pillars.
(4) Characterising pillar geometry.
(5) Computing the height and volume of the void inside galleries and extraction chambers.
(6) Computing the overburden thickness to the surface.

Importing the Dataset

All 1·11 billion 3D points delivered by the survey company came bundled in a single (compressed) LAZ file that most computers today will not read. Upon the authors' request, CloudCompare now includes a tiling feature to split large LAS/LAZ files into smaller manageable tiles with a tile-naming convention in column and lines counted from the bottom left of the image (Fig. 8).

Raw Point-cloud Visualisation

Zeb point clouds come as purely geometric data, without intensity. Visualisation with CloudCompare is highly improved with the eye-dome lighting (EDL) shader activated

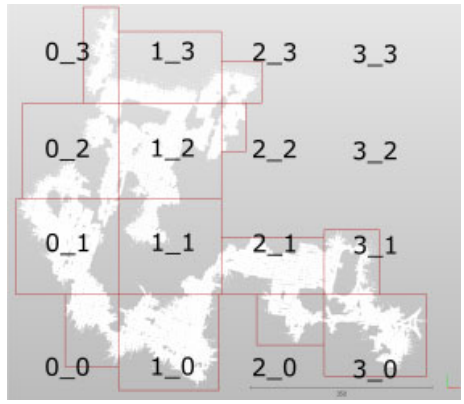

FIG. 8. Entire LAZ files can be tiled during import. File tiling indices follow this pattern. Blocks appear irregular because boundaries are adjusted to actual 3D points.

(Fig. 9). This shader enhances the view with dynamic, real-time, pseudo lighting to render the local relief. Relief rendering is a function of the point-cloud domain the shader acts on. Smaller extents reveal surface gradients better, whereas larger domains only express broader relief features (A in Fig. 9).

Indoors laser point clouds show the outer skin of galleries. To look inside them, the roof should be taken off (B in Fig. 9), which is achieved virtually by assigning the Z coordinate to a new scalar field and thresholding this elevation attribute. Alternatively, a viewer-based perspective display mode enables walking through galleries from the inside, much like in arcade video games (C in Fig. 9). Controlling the view may be tricky and requires some practice. The advantage of this view, however, is to place the observer back in the field position. It is very useful for revisiting the cavity after the survey and checking observations.

As is visible in B and C in Fig. 9, the Zeb operator, or field assistant, may show up in point clouds. While the laser scanner has a back plate, designed to create a shadow where the operator should hide, it is very difficult to always remain hidden during the journey. To filter these out, the ShadVis plugin implementing the *portion de ciel visible* (portion of visible sky – PCV), a technique derived from Tarini et al. (2003), may compute a useful scalar field. Since points reflecting off the operator are entirely contained inside the gallery volume, they will not receive any light from the outside. Thus, thresholding the lowest illuminance scores will exclude them from the point cloud. Beyond these initial processing steps, proper geotechnically oriented interpretation may start.

Gridding Point Clouds for Quarry Outlines and Ceiling and Floor Segmentation

Geographical information systems (GIS) today are still not really capable of handling hundreds of millions of 3D points, whereas CloudCompare handles them by design. However, many spatial analyses and geotechnical hazard mapping are optimally performed using GIS software. To bridge the best of both worlds, point clouds can be turned instantly into GeoTIFF grids with CloudCompare's Raster tool. For mapping purposes, the projection is obviously performed along the Z axis, but X or Y axes may also be chosen instead.

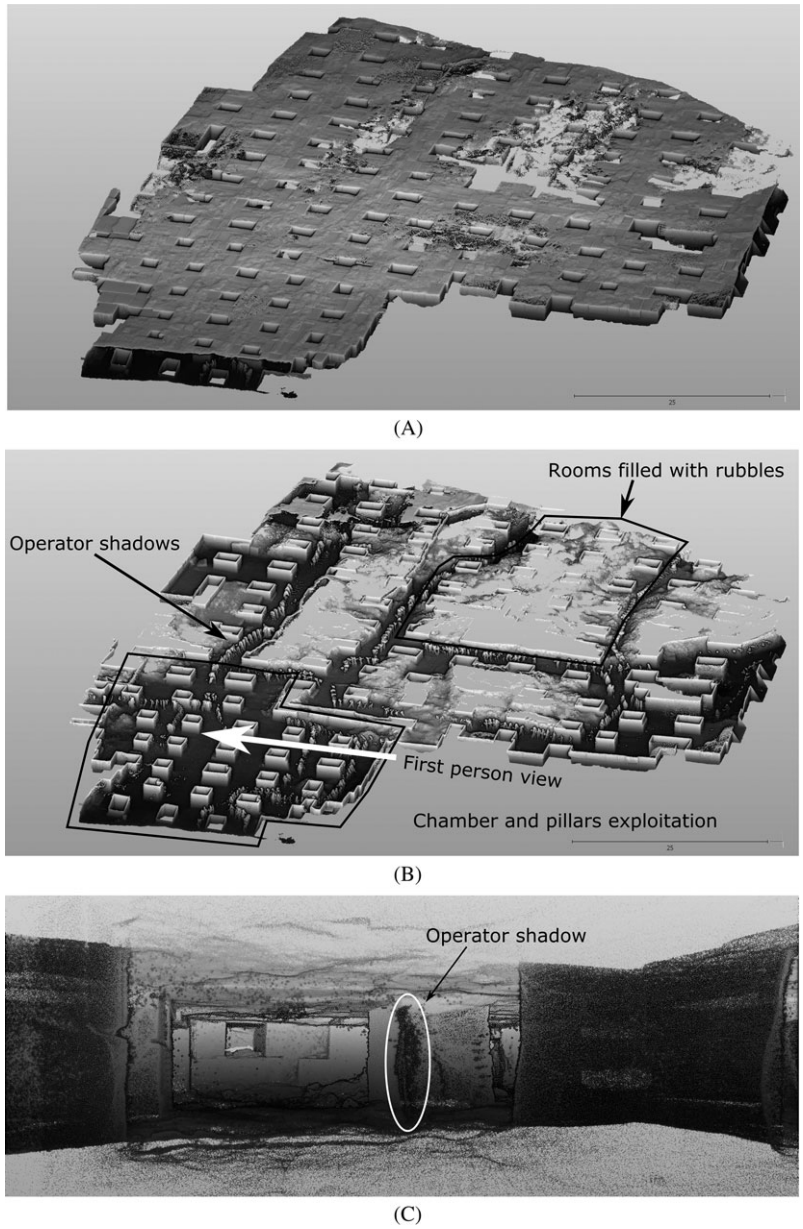

FIG. 9. (A) Quarry visualisation with eye-dome lighting shader enhancing local relief. (B) Same view with the quarry roof off – thresholding based on point elevation and non-applicable numbers (NaNs) such as out-of-range values or hidden points. The regular pillar geometry is immediately obvious. (C) Viewer-based perspective of a gallery as a first-person view. The view location is marked by a white arrow in B.

Rasterising point clouds means it is practical to extract: (i) gallery outlines in a GIS; (ii) gallery heights from the grid height range attribute; and (iii) gallery floor and roof geometry when attributing the minimum and maximum elevation value of points contained in each pixel. The underlying grid interpolation method is a nearest-neighbour approach. Empty cells can, optionally, be interpolated linearly.

Gallery Height

Geotechnically, gallery roof height is an item of information used to compute the maximum volume debris cone, given the rubble's angle of repose. A pillar's width-to-height ratio, partly conditioned by the gallery roof height, also controls the overall stability of the quarry. Gallery height is readily available at the gridding stage, under the *height range* attribute of grid points (Fig. 10). The height range attribute encodes the maximum range between the highest and lowest point in a grid cell, even though the corresponding geometric object carrying this information may be either the most elevated point in the grid cell, or the lowest if the elevation minimum is retained.

In Fig. 10, entire sectors of the quarry were filled with rubble. Some sectors suffered from roof collapse, but others were deliberately filled by quarry operators to stabilise extraction work. With little space left between the floor and ceiling, decompressed material that would happen to collapse from the roof would quickly occupy the available volume and self-stabilise the void. These shallow roof heights were surveyed with the Zeb-Revo mounted on a monopod.

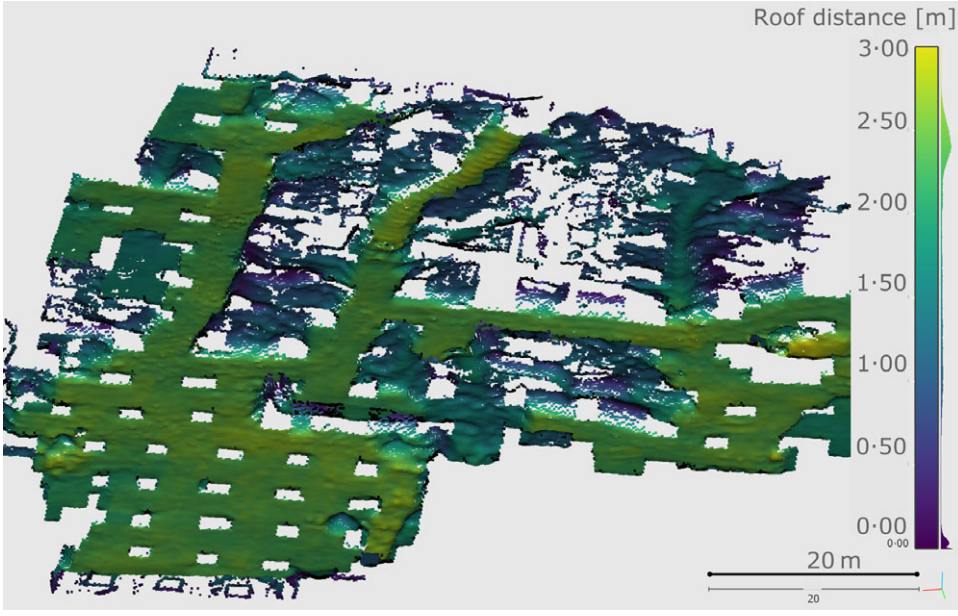

FIG. 10. Quarry floor obtained from gridding the original point cloud into 20 cm × 20 cm cells and retaining the minimum elevation. Colours depict the elevation range in each cell. Yellows indicate galleries about 2·40 m high. Green-blue shades mark chambers filled with rubble to prevent roof collapse.

An alternative method to classify ceilings, walls and floors also exists based on surface orientation, which preserves point-cloud density. It consists of classifying each point into a mutually exclusive floor, wall and ceiling class based on the point's local neighbourhood geometry, as described below.

FACETS: a Structural Geology Tool to Separate Walls from Floors and Ceilings

Gallery faces (floor, walls and ceiling) are characterised by specific orientations. Numerically, orientation is determined by computing the normal-vector parameters of the best-fitting local plane to each point, within a specified diameter. CloudCompare computes them in Edit > Normal > Compute, and may "guess" a realistic search diameter. To make normal parameters understandable, they may be exported as dip and dip-direction scalar fields.

In quarries or buildings, walls are (roughly) vertical objects, while floors and ceilings are somewhat horizontal. The plugin FACETS in CloudCompare is dedicated to structural geology and enables interactive exploration of point clouds based on local surface normal vectors (Dewez et al., 2016a). It implements an interactive stereogram tool (Fig. 11) where each point coordinate is plotted with its dip and dip-direction attribute in the upper hemisphere. Given the high redundancy of identical dip and dip-direction values, the stereogram colours translate as point density. This graph can be queried numerically or interactively by clicking anywhere in the stereonet space. Points excluded by the selection are dynamically turned off in the 3D view.

For the purpose of this research, wall points correspond to all points with a normal oriented with a dip within $70° \pm 20°$, at any azimuth (dip direction of $0° \pm 360°$). These points appear along the periphery of the stereonet (Fig. 11). On the other hand, the floor and ceiling are made of points with a vertical normal: they appear at the stereonet's centre in Fig. 11.

While walls directly come out of this segmentation, ceiling and floor points can only be extracted as a mixed point cloud. In this instance, because the quarry is only gently dipping 3° to the north-west (N287°E–03°NW), it is possible to fit a best-fitting plane

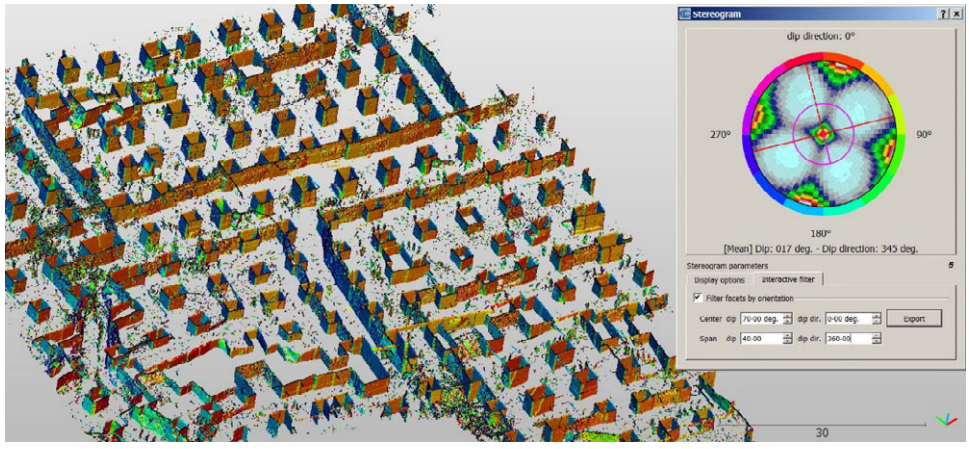

FIG. 11. Interactive cloud segmentation with CloudCompare's FACETS stereogram tool (Dewez et al., 2016a) based on dip and dip-direction pairs. Here, displayed points have dips of $70° \pm 20°$ (upper hemisphere plot in the inset). Note that *dip span* indicates the total range, not the half-span.

running between the ceiling and floor. The distance from the plane to the ceiling ought to be positive, while distance to the floor is negative.

The use of FACETS presented here is a by-product of its original intent (see Dewez et al., 2016a). Here it only makes use of point normals which have been computed beforehand and does not attempt to reconstruct planar facets.

Gallery Width

The last unknown gallery parameter needed to diagnose a roof-collapse hazard is the roof span between supports, for example, pillars and external walls of the quarry. This parameter determines the likely diameter of the circular collapse shaft that will reach the (outdoor) ground surface. CloudCompare's cloud-to-cloud distance between the wall and ceiling point clouds enables this computation. Alternatively, this operation can also be performed with standard GIS Euclidian distance grids from the pillars and walls mask grid. Fig. 12 is a demonstration using CloudCompare on a sample area.

Cavity Volume

Once floor and ceiling points have been tagged and split into two different clouds, CloudCompare can compute the volume between both surfaces as the integral of vertical prisms between both surfaces (an extension of the Raster tool). Over the extent of the test site (see Fig. 10), the 2·5D volume of the void, computed over 1 m² cells, equates to 4472 m^3 over an area of 5015 m². So even though some galleries reach about 2·40 m in height (Fig. 13), gallery height over the entire quarry sector averages only 0·89 m because rubble

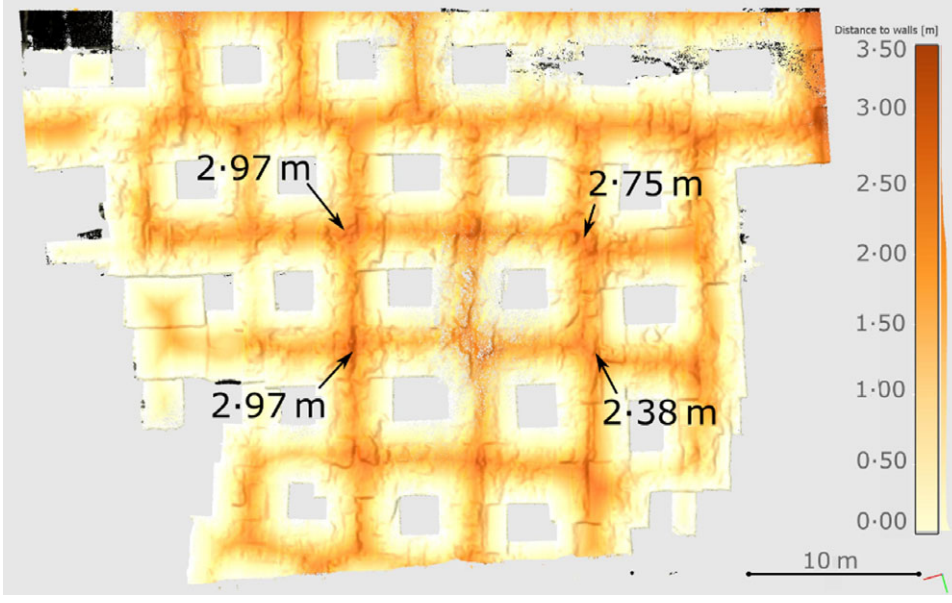

FIG. 12. Gallery width at ceiling level corresponding to the sector of Fig. 11. Gallery width was computed in CloudCompare as the cloud-to-cloud distance between wall points, taken as reference, and ceiling points.

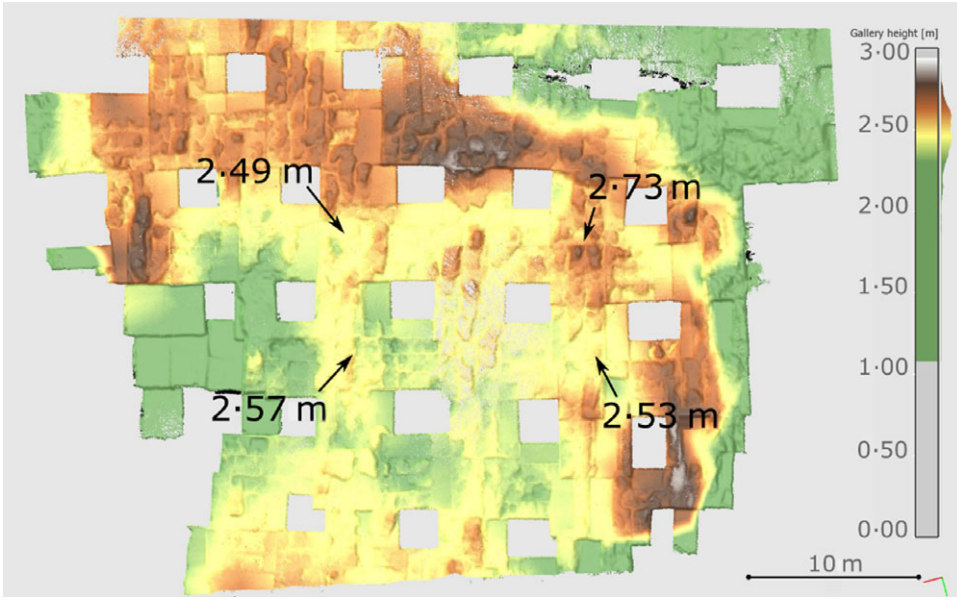

FIG. 13. Gallery roof geometry with the height-range attribute. Note the rough nature of the ceiling in the upper central part of the image, translating as potential locations of roof collapse.

fills large parts of the quarry. Room filling reduces the overall volume available for a generalised roof collapse.

DISCUSSION

Laser scanning holds tremendous potential for mapping underground cavities and reducing geometric uncertainties. Yet geometry is not the only ingredient required to produce a pertinent hazard map and handle cavity-collapse risks. Below is a discussion of the significant contributions, tracks for developments and key elements influencing the contribution of laser scanning to the field.

Risk Managers' Requirements

Until now, cavity-collapse risk-management decisions in France have been made on static 2D maps at a fixed scale. The hazard map is designed to support a regulatory risk mitigation plan known as the Plan de Prévention des Risques Cavités. Civil security managers take protective measures to protect people and goods based on them.

The choice of scale is a compromise between the spatial extent of the study area, the degree of knowledge of a hazard and its spatial variability, and the personnel and funding resources allocated to collect and aggregate data for a new cartographic document. At 1/5000 scale, the decision can be made very specifically at the parcel level, if the geometry can be trusted.

The geometric accuracy at 1/5000 scale, using national mapping agencies' usual rule of thumb, considers that any geometric information cannot be drawn on the map better than at

0·2 mm. At 1/5000 scale, 0·2 mm represents 1 m. Therefore, any point, line or polygon printed on the map can only depict objects to within 1 m.

What is a Handheld Laser Scanner Good At?

Geotechnical stability diagnostics depends on describing the global (location and dimensions) and local (wall and pillar integrity) geometry of a cavity. Handheld laser scanners enable complete dimensioning of cavities with gallery width, height, volume of voids, location of voids with respect to assets above ground and thickness of the overburden with an accuracy better than 1 m. The locational accuracy is entirely down to the co-registration process between loops and to the way the assembled point cloud is tied to an independent rigid network of control points. One trusts the professional surveyors appointed to perform this task, as they routinely do elsewhere, but the authors regret that they could not provide more factual data to document this.

Could these geotechnical parameters have been acquired by other means? Heights and widths could be documented with a total station survey, but with far fewer key points (tens to hundreds of thousand times less) than the 1·1 billion 3D points of this laser scanner survey. However, the sheer size of the task makes this uneconomic. In the surveyed section of the quarry in this paper, which is only 10% of the total quarry size, 1964 pillars of more than 2 m^2 were mapped in four days. For an equivalent survey with a total station, each pillar would require 8 points to define their prismatic shape (thus more than 15 000 sightings) and probably hundreds of stations to view all sides of the pillars. Survey time means cost. Even though handheld laser surveys produce hundreds of millions of points, many of which are admittedly irrelevant for 1/5000 quarry outline mapping, they are the only economical solution available at the present time.

Previous studies put time gain as the primary reason to perform handheld laser scanning. James and Quinton (2014) claim that handheld mobile scanning is about 40 times faster than conventional TLS, and six times faster than SfM photogrammetry in outdoor conditions (saltmarsh creek and cliff surveys). Eyre et al. (2016), in a mining environment, identified that handheld mobile scanning surveys were about eight times faster at the field survey stage (half an hour versus half a day of survey). They also point to the performance at the processing stage, where the SLAM computation takes about the same time as survey loops, while terrestrial laser scanner surveys take considerably more post-processing time for piecing scan stations together.

Point density was also noted as useful by Eyre et al. (2016) for documenting fractures with an accuracy of $4{\cdot}5° \pm 2{\cdot}6°$ from terrestrial laser surveys, a limit caused by noisy points. These authors also note that fracture mapping from Zeb point clouds was partially inefficient for shallow-angled fractures where surface expressions are small. Here, comparatively sparse point density combined with point measurement noise are the culprit. Since these fractures are the most threatening features for gallery collapse, geotechnical engineers should keep an eye specifically on these elusive features when performing their stability diagnostic. Thus, not all fractures will be visible in the point cloud.

Finally, in an era where quality norms impose a requirement to trace processes such as the ISO 9001 quality management norm, point clouds can be tangible documents to support collegial expert decisions. Bringing a group of experts underground is never truly feasible, but reviewing extremely realistic underground representations from the comfort of a meeting room after a survey may lead to better decisions. For this assertion to be true, however, software and visualisation tools (as in evocative techniques but also remote viewing capabilities) must still be significantly improved.

What can Handheld Mobile Laser Scanners Not Do, or Do Imperfectly?

As already underlined, handheld laser scanners absolutely need a backbone of control points surveyed by a total station to tie into. Zeb surveys are no different to any other survey traverse tools. Adjustment and external control must bring confidence. In their absence, ventilation shafts visible at the outdoor ground surface may often serve to check the global georeferencing of underground galleries. However, they may not be sufficiently abundant or well distributed to provide the necessary control. Handheld laser scanners do not replace traditional surveying tools, they complement them.

Conclusion

The Zeb-Revo handheld mobile laser scanner was tested in both indoor and outdoor conditions for the purpose of mapping underground cavities. Outdoors, the scanner's range did not exceed 7·5 m for 99% of points. Indoors, it reached up to 30 m and on one occasion 35 m. Planar surface reconstruction at ranges shorter than 10 m possessed a RMS better than 10 mm. Horizontality was unbiased up to a baseline of 32 m. Defects in point-cloud rigidity could not be demonstrated for surfaces measured 5·25 minutes apart. Their interval distance was accurate to within 3 mm over 30·20 m, a relative accuracy of 1/10 000.

Over large sites, Zeb surveys occur in loops combined as traverses. Registration quality is down to feature matching, iterative-closest-point solution algorithms and traverse adjustment. In the survey of a large underground quarry extending over 11 ha, all 25 loops, surveyed over four working days, successfully closed to a conventional survey station network with a referencing error lower than 1 m, and mostly with a residual error smaller than 10 cm. Such residual errors are acceptable for hazard mapping at 1/5000 scale.

Point clouds generated with the Zeb-Revo had a median point density of 1 point/21 mm, which is more than sufficient to locate walls and pillars, determine the height and width of galleries, and depict roof-collapse features and the main fractures. CloudCompare, as free point-cloud manipulation software, was adopted to import over 1 billion laser points in tiles as LAS/LAZ files. In addition, it contains most of the tools necessary to prepare GIS information layers for entry into existing cavity-collapse diagnostics pipelines.

Today, given the performance of the Zeb-Revo, handheld laser scanners alleviate the geometric challenge of cavity hazard mapping. Now, uncertainties are down to rock-mass characteristics, but this is beyond the scope of the authors' profession.

Acknowledgements

The quarry survey was carried out by the Paris-based surveying company Geoperspectives. GeoSLAM is thanked for their responsive technical support. The authors wish to thank Clara Lévy and Florian Masson for insightful comments and discussions. Thomas Dewez's research time was partly funded by the Institut Carnot BRGM mobility grant project RADIOGEOM at Uni Research in Bergen, Norway.

References

Baiden, G., Bissiri, Y., Luoma, S. and Heinrich, G., 2014. Mapping utility infrastructure via underground GPS positioning with autonomous telerobotics. *Tunnelling and Underground Space Technology*, 39: 6–14.

Besl, P. J. and McKay, N. D., 1992. A method for registration of 3-D shapes. *IEEE Transactions on Pattern Analysis and Machine Intelligence*, 14(2): 239–256.

Bosse, M., Zlot, R. and Flick, P., 2012. Zebedee: design of a spring-mounted 3-D range sensor with application to mobile mapping. *IEEE Transactions on Robotics*, 28(5): 1104–1119.

Buckley, S. J. and Mitchell, H. L., 2004. Integration, validation and point spacing optimisation of digital elevation models. *Photogrammetric Record*, 19(108): 277–295.

Cadge, S., 2017. Cave surveying with the GeoSLAM Zeb-Revo. *BCRA Cave Radio and Electronics Group Journal*, 97: 3–5.

Chan, T. O., Lichti, D. D., Belton, D., Klingseisen, B. and Helmholz, P., 2016. Survey accuracy analysis of a hand-held mobile LiDAR device for cultural heritage documentation. *Photogrammetrie – Fernerkundung – Geoinformation*, 3: 153–165.

CloudCompare, 2015. http://www.cloudcompare.org/doc/wiki/index.php?title=Roughness [Accessed: 3rd October 2017].

Dewez, T. J. B., Rohmer, J., Regard, V. and Cnudde, C., 2013. Probabilistic coastal cliff collapse hazard from repeated terrestrial laser surveys: case study from Mesnil Val (Normandy, northern France). *Journal of Coastal Research, Special Issue*, 65(1): 702–707.

Dewez, T. J. B., Girardeau-Montaut, D., Allanic, C. and Rohmer, J., 2016a. FACETS: a CloudCompare plugin to extract geological planes from unstructured 3D point clouds. *International Archives of Photogrammetry, Remote Sensing and Spatial Information Sciences*, 41(B5): 799–804.

Dewez, T. J. B., Leroux, J. and Morelli, S., 2016b. Cliff collapse hazard from repeated multicopter UAV acquisitions: return on experience. *International Archives of Photogrammetry, Remote Sensing and Spatial Information Sciences*, 41(B5): 805–811.

Eyre, M., Wetherelt, A. and Coggan, J., 2016. Evaluation of automated underground mapping solutions for mining and civil engineering applications. *Journal of Applied Remote Sensing*, 10(4): article 046011.

Gallay, M., Hochmuth, Z., Kaňuk, J. and Hofierka, J., 2016. Geomorphometric analysis of cave ceiling channels mapped with 3-D terrestrial laser scanning. *Hydrology and Earth System Sciences*, 20: 1827–1849.

Geoderis, 2006. Qualification de l'aléa fontis: méthodologie pour le bassin ferrifère lorrain, Géoderis e-2006/320DE-06LOR2500. 52 pages. http://www.grand-est.developpement-durable.gouv.fr/IMG/pdf/Telecharger_le_rapport_GEODERIS_de_gradation_de_l_alea_fontis_septembre2006_cle21bafc.pdf [Accessed: 4th December 2017].

Hannemann, W., Brock, T. and Busch, W., 2012. Zustandsdokumentation ausgedehnter untertägiger Hohlraumsysteme. *Photogrammetrie – Fernerkundung – Geoinformation*, 6: 691–700.

Heitfeld, M., Kluener, J., Mainz, M. and Schetelig, K., 2006. Risk of collapse features from near-surface cavities in old mining cities. The Geological Society of London 10th IAEG International Congress, Nottingham, UK. Paper 461, 13 pages.

Hokuyo, 2017. *Specifications of Hokuyo UTM-30LX*. https://www.hokuyo-aut.jp/search/single.php?serial=169 [Accessed: 3rd October 2017].

IFSTTAR, 2014. *Le diagnostic de stabilité des carrières souterraines abandonnées: guide méthodologique*. IFSTTAR publication C1502617, Champs sur Marne, Paris, France. 105 pages. http://www.ifsttar.fr/fileadmin/user_upload/editions/lcpc/GuideTechnique/GuideTechnique-LCPC-DIAGCAR.pdf [Accessed: 3rd October 2017].

James, M. R. and Quinton, J. N., 2014. Ultra-rapid topographic surveying for complex environments: the hand-held mobile laser scanner (HMLS). *Earth Surface Processes and Landforms*, 39(1): 138–142.

Langer, W. H., 2001. Potential environmental impacts of quarrying stone in karst – a literature review. *US Geological Survey Open-File Report, OF-01-0484*. US Department of the Interior and US Geological Survey. 39 pages.

Musialski, P., Wonka, P., Aliaga, D. G., Wimmer, M., van Gool, L. and Purgathofer, W., 2013. A survey of urban reconstruction. *Computer Graphics Forum*, 32(6): 146–177.

Roncella, R., Umili, G. and Forlani, G., 2012. A novel image acquisition and processing procedure for fast tunnel DSM production. *International Archives of Photogrammetry, Remote Sensing and Spatial Information Sciences*, 39(B5): 297–302.

Tarini, M., Cignoni, P. and Scopigno, R., 2003. Visibility based methods and assessment for detail-recovery. *IEEE Visualization Conference*, Seattle, Washington, USA. Pages 457–464.

Thiele, S. T., Grose, L., Samsu, A., Micklethwaite, S., Vollgger, S. A. and Cruden, A. R., 2017. Rapid, semi-automatic fracture and contact mapping for point clouds, images and geophysical data. *Solid Earth*. Discussion paper, https://doi.org/10.5194/se-2017-83, in review, 2017. [Accessed: 4th December 2017].

Vanneschi, C., Eyre, M., Francioni, M. and Coggan, J., 2017. The use of remote sensing techniques for monitoring and characterization of slope instability. *Procedia Engineering*, 191: 150–157.

VUIDART, L., 2012. Guide technique pour l'homogénéisation des études détaillées des aléas miniers: volet effondrement localisé, Rapport GEODERIS N2012/010DE – 12NAT2210. http://www.geoderis.fr/ [Accessed: 4th December 2017].
ZLOT, R. and BOSSE, M., 2014. Efficient large-scale three-dimensional mobile mapping for underground mines. *Journal of Field Robotics*, 31(5): 758–779.

Résumé

Les cavités souterraines sont légions dans le sous-sol urbain et rural d'Europe du nord du fait de sa longue histoire minière et sa croissance urbaine. La gestion du risque d'effondrement de cavités demande une connaissance aussi exacte que possible de la localisation des cavités, de leurs dimensions et d'éventuels facteurs aggravants. Les techniques de cartographies actuelles ne sont soit pas assez exactes, ou détaillées soit encore pas économiquement viables. Dans cette étude un scanner laser portable à la main, GeoSLAM Zeb-Revo, est testé. Les nuages de points reproduisent les plans avec une erreur de moins de 10 mm (EMQ) pour des portées typiques de galeries souterraines (<10 m). Les levés ne souffrent pas, de manière mesurable, de déviations de la verticale. Un test de distance, pour des conditions de dérive instrumentales de 5,25 minutes au bout d'un parcours de 115 m, reproduit une base de 30 m avec une erreur, non significative, de 3 mm (1/10 000). Appliqué à 11 ha de carrière souterraine de pierre de construction dans le Bassin Parisien (Nord de la France), le levé Zeb-Revo, composé de 25 boucles co-registrées entre elles, a une exactitude meilleure que 1 m. Ce niveau d'exactitude est compatible avec l'établissement de carte d'aléa d'effondrement au 1/5000. Dorénavant, les incertitudes des cartes d'aléa d'effondrement ne sont plus tributaires que de l'incertitude de la qualité de la roche, la technologie laser portable supprime l'incertitude géométrique qui persistait à ce jour.

Zusammenfassung

Unterirdische Hohlräume sind in vielen nordeuropäischen Städten und ländlichen Gebieten sehr verbreitet, wegen der langen, historischen Entwicklung des Bergbaus und wegen dem Abbau von Naturbausteinen. Um die Risiken von Einstürzen solcher Hohlräume einzuschätzen, bedarf es detaillierter Informationen über die Geometrie, die Tiefe und die Charakteristik der Gesteinsmassen. Für die Kartierung dieser unterirdischen Hohlräume werden aktuell Verfahren eingesetzt, die weder ausreichend genau und detailliert, noch kosteneffektiv sind. In diesem Umfeld wurde ein mobiler Handlaserscanner GeoSLAM Zeb-Revo getestet. Die damit erfassten Punktwolken reproduzierten die Ebenen über die typischen Dimensionen solcher Galerien (<10 m) wirklichkeitsgetreu (RMS< 10 mm) und es konnten keine Kippachsenfehler festgestellt werden. Handelt es sich um gut strukturierte Netzwerke von Gängen, konnte nach einer Schleife von 115 m und 5·25 Minuten mit instrumenteller Drift eine maximale Abweichung von 3 mm auf 30 m (1/10 000) erzielt werden und die Differenz zur Solllänge war unerheblich. Für ein größeres Projekt mit 11 ha eines aufgegebenen unterirdischen Steinbruchs im Pariser Becken ergab die Vermessung mit Zeb-Revo genaue (<1 m) Karten, die für behördliche Gefahrenkarten im Maßstab 1/5000 geeignet waren. Damit stellt die Geometrie keine Herausforderung mehr dar, um Gefahrenkarten für diese Objekte zu erstellen.

Resumen

Las cavidades subterráneas son abundantes en el subsuelo urbano y rural del norte de Europa debido a su larga historia minera y al crecimiento urbano. La gestión del riesgo de colapso de una cavidad requiere un conocimiento tan preciso como sea posible de la geometría, la profundidad y la caracterización de la masa de rocas. Las técnicas usuales de medida no son lo suficientemente precisas, detalladas ni rentables en entornos subterráneos. En este estudio, se prueba un escáner láser de mano, GeoSLAM Zeb-Revo. Sus nubes de puntos

reproducen los planos con un error menor de 10 mm (RMS) en dimensiones típicas de galerías (<10 m). Los errores en medidas horizontales no son apreciables. En las redes de medida bien estructuradas en galerías, el error de la distancia de referencia no superó los 3 mm sobre 30 m (1/10 000) después de un bucle de 115 m y 5,25 minutos de deriva instrumental. Y la diferencia con respecto a la longitud de referencia fue insignificante. Aplicado a la cartografía de 11 ha de una cantera de piedra subterránea en desuso en la Cuenca de París, las medidas de Zeb-Revo produjeron mapas de base precisos (<1 m) adecuados para mapas de riesgos de colapso de cavidades a escala 1/5000. El conocimiento geométrico de las cavidades accesibles, por lo tanto, ya no es un desafío para la generación de mapas de riesgo de colapso.

摘要

由于开采矿产和建筑石材的悠久历史,北欧的城市和农村遍布地下洞穴。洞穴塌陷风险的管理需要详细了解洞穴的几何形状、深度和岩石特性。当前的地图测绘方法在地下环境中既不够准确、详尽,也不具成本效益。本研究测试了GeoSLAM Zeb-Revo手持可携式激光扫描仪,其获取的点云数据在常见的通道距离(<10米)内实现了高精度的平面量测(RMS<10毫米),而且在量测的范围内没有发现任何水平缺陷。在结构良好的廊道网络内,115米环路测量在5·25分钟仪器漂移后相对距离误差为1/10 000,亦即30米不超过3毫米,与参考值差异不大。应用Zeb-Revo于巴黎盆地测绘11公顷废弃的地下采石场,生成精确的(误差<1米)的地图,适用于制作1/5000比例尺的洞穴风险地图。由此,对于可达洞穴的几何信息获取以生成塌陷危险地图不再是项挑战。